ELSEVIER

Biochimica et Biophysica Acta 1458 (2000) 120–134

BIOCHIMICA ET BIOPHYSICA ACTA
BBA

www.elsevier.com/locate/bba

Review

Biophysical aspects of intra-protein proton transfer

Sharron Brandsburg-Zabary *, Orit Fried, Yael Marantz, Esther Nachliel, Menachem Gutman

Laser Laboratory for Fast reactions in Biology, Biochemistry, Tel Aviv University, Tel Aviv, Israel

Received 1 November 1999; accepted 1 December 1999

Abstract

The passage of proton trough proteins is common to all membranal energy conserving enzymes. While the routes differ among the various proteins, the mechanism of proton propagation is based on the same chemical–physical principles. The proton progresses through a sequence of dissociation association steps where the protein and water molecules function as a solvent that lowers the energy penalty associated with the generation of ions in the protein. The propagation of the proton in the protein is a random walk, between the temporary proton binding sites that make the conducting path, that is biased by the intra-protein electrostatic potential. Kinetic measurements of proton transfer reactions, in the sub-ns up to μs time frame, allow to monitor the dynamics of the partial reactions of an overall proton transfer through a protein.

Keywords: Proton transfer; Diffusion; Electrostatic potential; Ion conductive channel; Microcavity

1. Introduction

In the present paper, we wish to elaborate on the mechanism of proton transfer within proteins, a mechanism that is common both in proton pumping protein and in proton-driven enzyme transporters or other $\Delta\mu H$-driven systems. From a biochemical point of view, the translocated protons may be products of redox reactions, scalar protons or vectorial pumped protons. From a biophysical point of view, these processes are based on the same mechanism. Due to its high charge density and solvation energy, a proton will not be readily inserted into the low dielectric constant matrix of a protein, unless there is an appropriate compensation by some structural rearrangement or covalently bound to an anionic site. The stabilization of the proton in the protein is only the first step in the pumping mechanism; the proton has to re-dissociate and reacts with one or many sites until it crosses the protein and is released to the bulk on the other side. In the present paper, we shall regard proton pumping as a sequence of dissociation, diffusion and rebinding steps. In accordance with this mechanism, the manuscript will focus on the mechanism of the partial events; the dissociation, the diffusion and what are the forces that convert a channel into an efficient pump.

2. Mechanism of proton dissociation

The dissociation reaction is the first step in any proton transfer reaction whether it proceeds in aqueous solution or inside a protein. The dissociation of an acidic residue to a proton plus a conjugated base

* Corresponding author. Fax: +972-3-6415053.

0005-2728/00/$ – see front matter
PII: S0005-2728(00)00063-3

is a function of the surrounding solvent. As the moiety dissociates into a ion pair, the electrostatic energy of the system increases. Thus the solvation of the products should be energetically sufficient to compensate for the incremental self-energy of the system. For proton dissociation at the protein's surface, there are ample water molecules to stabilize the products. Inside a protein, both the intra-protein water molecules and the protein itself function as a part of the stabilizing system. For this reason, we find that the initial step in proton pumping by bacteriorhodopsin calls for the anionic moieties of D85 to be present at the right position and distance from the Schiff base. Replacement by a non-protonable moiety like in the D85N or a shorter residue (D85E) already modifies the efficiency of the reaction [1–3].

The studies of proton transfer inside a cavity necessitate dynamics measurements. The role of the local environment of a protein in the solvation of the proton cannot be attained by equilibrium measurements, as they would sum both intra-cavity and cavity to bulk energetic terms. Thus the capacity of a small cavity in a protein to stabilize a proton has to be studied at a sub-ns resolution as attained by the laser-induced proton pulse [4–9].

The technique of the laser-induced proton pulse has recently been reviewed [5,10,11], thus it will be described very briefly. The essence of this experimental method is a synchronized excitation of hydroxy-aromatic compounds to their first electronic singlet state, which is much more acidic than the ground state [5,12–16]. The whole cycle of excitation, dissociation and relaxation to the ground state lasts only a few ns. The dissociation dynamics can be measured either in the excited state using sub-ns time-resolved fluorescence [13–15] or for the ground state reactions, by spectrophotometric monitoring of the state of protonation of pH indicators [9]. The results of the observed dynamics are subjected to a rigorous kinetic analysis [13,17] that yields the rate constants of all reactions involved in the overall process. The time-resolved fluorescence measurements provide the rate constant of the dissociation reaction, that of the recombination, the diffusion coefficient of the proton in the immediate solvent and the intensity of the electrostatic field in the reaction space. Transient absorption measurements yield the second order rate constants of all proton transfer reactions and the accessibility of protons and the pyranine anion to the various sites of the protein.

The water molecules in small cavities, like the heme binding site of apomyoglobin, are a poor solvent. In such an environment, the water molecules in the cavity are tightly bound to the residues forming the enclosure and cannot stabilize the dissociating proton at a rate compatible with the frequency of the dissociation attempts. As seen in the first column of Table 1, the dissociation rate of pyranine varies with the environment, ranging from 7×10^9 s^{-1}, as in multilamellar structures made of PC and PS, down to 2.2×10^8 s^{-1} in the heme binding site of apomyoglobin. The modulation of the dissociation rate is attributed to the kinetic incompetence of the water molecules; in most attempts, the proton will fail to be solvated and relax to the bound state. In well hydrated spaces, like in the porin channel or in the aqueous layer between phospholipids structures, the water molecules are more abundant and the solvation is faster. These considerations imply that the effective acidity of a residue in a protein is determined by its local environment. While this statement is generally affirmed by equilibrium studies, the measured parameters are summing both the intra-cavity plus the cavity to bulk equilibria. Only the time-resolved kinetics can focus on the intra-cavity reactions.

The calibration of the solvent's capacity to stabilize the products had been achieved by measuring the kinetics of proton dissociation in concentrated salt solutions of known activity of the water. These kinetic measurements revealed that rate of dissociation decreased with the activity of the water according to the empirical expression: $k_i = k_0(a_{H_2O})^{-n}$. The term k_0 is the rate constant measured in pure water, while n is an empirical number that is characteristic of the dissociating molecule ($4 < n < 10$) [10,18–24]. Based on this relationship, the equivalence of intra-protein cavities or the space between lipid surfaces was measured and the results are listed in Table 1.

3. The effect of solvent on proton diffusion

During the catalytic cycle of proton pumping proteins, the proton has to enter and propagate through the conducting channel. Each step along its way is a

translational diffusion between adjacent sites, while at each site the process of dissociation and recombination events repeatedly takes place. To provide an efficient proton conducting channel, the protein must decorate the channel walls with moieties that can act as reversible proton acceptors; carboxylates, histidine moieties or stretches of water molecules that are sufficiently free to interact with the proton along its way. The carboxylate and water molecules in the bacteriorhodopsin conducting channel [3,25] or the glutamate of the cytochrome oxidase, 'D pathway' [26–28], demonstrate the necessity of the continuation of proton-solvating sites to ensure the efficient propagation of the proton along the channel.

The diffusion of proton in water proceeds by the Grotthuss mechanism [29]. Free protons exist in aqueous solution either as fully solvated H_3O^+ or $H_5O_2^+$. The former is characterized by a planar geometry of the H_3O^+ species and its capacity to form hydrogen bonds through the tree hydrogen atoms (the oxygen atom of the hydronium does not form a hydrogen bond). The $H_5O_2^+$ ion, also referred to as Zundel ion, can be readily detected by its specific IR signature; a wide absorption band (continuum) reflecting the manifold frequencies of the proton shuttling between the two water molecules flanking the excess proton [30,31]. The second solvation shell further stabilizes both structures and by its random fluctuations generates the mechanism that keeps the protonic charge in motion. The two states of the proton are in rapid equilibrium, thus when the proton is shifting its solvation state from $H_5O_2^+$ to H_3O^+, a diffusional step equal to the O–O separation distance is made (2.5 Å [32]). The driving force for shifting of the locus of the extra proton from one state to the other is the random motion of water molecules of the second solvation shell. For this reason, any reduction in the random motion of the water molecules of the solvent will suppress the diffusivity of the proton. This effect had been demonstrated in small cavities either in protein or in stable phospholipid structures (see Table 1) [18,19,22,24]. In these cavities, the enhanced interaction of the water molecules with the surface reduced their rotational freedom coupled with suppression of the proton diffusivity. Examination of the results points out that the nature of the enclosing matrix affects the diffusion coefficient. In small enclosures within a protein, the diffusion of a proton is $\sim$50% of that in bulk water, while water molecules surrounded by phospholipids are characterized by a higher diffusion coefficient (see Table 1). This observation may point that the immobilization of the water in the first solvation shell at the surface of a protein is more in-

Table 1

Site	κ_f (s^{-1})	a_{H_2O}	ε_{app}	$D_{H>+}$	Reference
water	7×10^9	1.0	78	9.3×10^{-5}	
Proteins					
apomyoglobin (heme binding site)	0.22×10^9	0.6	8	4.5×10^{-5}	[18]
lysozyme (anion binding site)	2.8×10^9	0.88	13.5	4.0×10^{-5}	[22]
PhoE (anionic channel)	5.5×10^9	0.966	24	4.0×10^{-5}	[19]
phospholamban (Ca^{2+} channel)	2.1×10^9	0.86	23	4.0×10^{-5}	[a]
Phospholipid structures					
Hex $II_{(DOPE+DOPC)}$ $d_w = 8$ Å	3.0×10^9	0.9	21	$8–9\times10^{-5}$	[b]
$multilamellar_{(DOPE+DOPC)}$ $d_w = 11$ Å	1.25×10^9	0.8	23	$8–9\times10^{-5}$	[b]
$multilamellar_{(PC)}$ $d_w = 11$ Å	1.2×10^9	0.77	38	$8–9\times10^{-5}$	[24]
$multilamellar_{(PC+cholesterol)}$ $d_w = 11$ Å	1.2×10^9	0.77	42	$8–9\times10^{-5}$	[24]
$multilamellar_{(DPPC)}$ $d_w = 11$ Å	2.5×10^9	0.86	50	$8–9\times10^{-5}$	[24]
$multilamellar_{(PC+PS)}$ $d_w = 55$ Å	7.0×10^9	1.0	49	9.3×10^{-5}	[24]
submitochondrial vesicles	2.7×10^9	0.87	20	2.3×10^{-5}	[23]

Compilation of physical and chemical characteristics of microcavities in proteins and phospholipid structures. For the lipid structures, d_w represents the repeating spacing of water between the lipid interfaces. κ_f: rate constant of proton discharge into the first solvation shell. ε_{app}: the dielectric constant of a homogeneous continuum that generates an electrostatic potential gradient suitable for simulation of the observed dynamics.

[a] Zabary-Bransburg, S., unpublished results.

[b] Fried, O., Ph.D. thesis.

tensive than at the phospholipid interface. When the environment drastically suppresses the freedom of the water molecules, as in the single file of water molecules within the gramicidin channel, the diffusion coefficient of the proton falls down to 3% of the bulk value [5,33–35]. The reduced diffusivity of the proton in the gramicidin channel is a direct consequence of the strong interaction of the dipoles of the peptide chain with the water molecules. When the proton in the channel assumes the state of the Zundel ion, electro-restriction pulls the two flanking water molecules towards the center. On the other hand, the flanking water molecules are held in position by the fixed dipoles of the peptide chain, preventing the rest of the water molecules in the channel to participate in the electro-constriction. Due to this 'anchoring', a gap is formed between the Zundel ion and the rest of the water molecules. This loss of connectivity is the cause for the reduced diffusivity of proton in the gramicidin channel.

The propagation by diffusion is the fastest mode for mass transfer over very short distances. The time interval needed for a proton to diffuse by random walk the whole length of the gramicidin channel, even at the reduced diffusion coefficient, is $\sim$15 ns. This time frame is orders of magnitude shorter than most catalytic even of fast proton pumping proteins like cytochrome oxidase. Thus in order to block a channel from becoming a proton leaking site, either the connectivity should be broken or that electrostatic potential field participates in forming barriers that prevent the passage of charges.

The crucial role of the aqueous phase continuity is evident from the mechanism of proton passage from the cytoplasmic face of the bacteriorhodopsin towards the Schiff base. No proton transfer takes place until the F helix is displaced from its original position in the M state of the protein, enhancing the solvation of the cytoplasmic facing section of the proton conducting channel [3,25]. The bacteriorhodopsin system also exemplifies the role of electrostatic potential in driving a proton translocation in a protein. Once the cytoplasmic section of the channel is solvated, the intra-channel carboxylate (D96) can be ionized and its electric charge acts as electrostatic attractor for protons ensuring its re-protonation by proton from the cytoplasmic matrix of the bacterium. Thus we cannot discuss the passage of proton in a protein without considering the electrostatic potential inside the channel.

4. Local electrostatic potential

The electrostatic forces within a protein are made up by the partial charges of intra-protein residues, surface charges, dipoles of the peptide bonds and the external field. The low dielectric constant of the protein together with the shape of the intra-protein cavities and the short distances make the electrostatic potential and its gradient to be extremely intensive [36]. For example, when the pyranine anion is inserted into the heme binding site of apomyoglobin, its charge is neutralized by the intra-cavity residues to $Z_{net} = -1$ [18]. Still its Coulomb cage radius (the distance where the electrostatic potential of the proton is equal to the thermal energy) was measured to be $\sim$70 Å, meaning that its electrostatic field expands out of the cavity.

The low dielectric constant of the protein matrix allows the electrostatic potential to propagate over a long distance, coupling the charge translocation with pK shifts at remote sites. The best studied examples for that long range coupling are the linkage of the electron transfer and proton transfer in the Q_A and Q_B domains of the reaction center [37–43]. Following a photo-excitation, the special pair of the reaction center ejects an electron into the cytoplasmic side of the protein forming the first stable reduction Q_A^-. The one electron-reduced quinone has to be stabilized in order to prevent rapid recombination of the electron with the oxidized special pair. This stabilization is gained by raising the pK of surface groups leading to their incremental protonation. Proton uptake measurement done on several mutants of reaction center showed that even groups located 17 Å from the Q_A^- site such as GluL212 are influenced by the extra charge and participate in its stabilization [44]. The reaction of the proton binding sites in the Q_A and Q_B domains with protons coming from the bulk partially compensates for the electron charge on the quinone. The Q_A^- state is only an intermediate and the electron propagates further on to a second quinone molecule (Q_B) located in a more solvated domain of the protein. The reduction of Q_B initiates a similar pK shift of the proton binding sites in its

defined domain as was measured by proton uptake experiments [45–47] and by theoretical calculation [48,49]. The protonation of the Q_B domain renders it to be stable enough to retain the electron from reacting with the oxidized special pair ($\tau \sim 10$ s). Reduction of the special pair by cytochrome *c* and absorption of a second photon initiates another round of electron transfer reactions which ends by the formation of the two electron-reduced Q_B. The two electron reduction of the quinone is terminated by the uptake of two protons and the QH_2 is released from the protein. Thus in the reaction center system, there are two types of proton transfer reactions. One is associated with the p*K* shifts caused by redistribution of electrons. The second one is the net migration of the proton into the reduced Q_B in order to generate the QH_2 species.

The protonation of the reduced Q_B is carried out through four co-existing intra-protein protonic channels [38]. The pathways are made of polar intra-protein residues and a few tens of water molecules [38,43] that enjoy some internal flexibility. Mutations that knock out an essential proton conducting element can be bypassed through another mutation within the domain [50–52]. On relating the rate of the electron transfer with the pH of the solution, it was noticed [37,53] that the protonation step was faster than the electron transfer, indicating that the protons were always available for the quinone in order to accept the coming electron. The time constant measured for the protonation was shorter than what was expected on the basis of diffusion-controlled reaction of protons with the domain. On this ground, it was concluded [37,38] that the proton sources for the formation of QH_2 were intra-protein protons, stored on the protonable moieties within the domain. This subject, of local proton reservoir, will be expanded below.

The p*K* shifts, caused by the appearance of the electron charge on the quinone, are difficult to measure. Such p*K* shifts, theoretically predicted on the basis of electrostatic calculations, impose technical limitations especially when the responding residues have a p*K* in the region where the protein is not stable any more. Monitoring a p*K* shift of a carboxylate residue, having a p*K* around 4–5, calls for lowering the pH of the solution up to a point where the protein might denaturate. Even if the protein can survive the treatment, the gradual protonation of the protein during its acidification affects the total charge, alters the p*K*, the very same parameter that is to be measured. Thus the acidimetric titration fouls the results. To measure the effect of charge increment on the p*K* of surface groups, the protein should be probed by a single proton, a reaction that can be attained only by a reversible single proton probing of the protein.

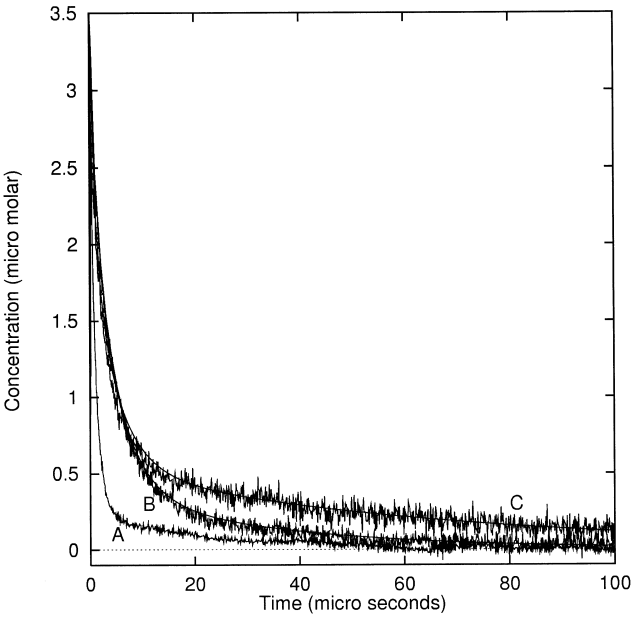

Fig. 1. Dynamics of pyranine re-protonation after pulse excitation of 20 μM pyranine. The measurements were carried out at pH = 7.4 in 100 mM NaCl (curve A) and 9 μM cytochrome *c* either in the oxidized or reduced states (curves B and C, respectively). Please note that the relaxation of curve C initiates with the same velocity as B but it trails in the longer time scale indication that the reduced protein can better retain its bound protons than the oxidized cytochrome *c*. Data from [54].

In the proton pulse experiment, the protein solution together with pyranine is pulsed by intensive laser pulses which release proton from the pyranine. The protons react with all proton binding sites in the system and their availability to react with the pyranine anion (taken as the reference reaction) is monitored by a continuous follow-up of the pyranine state of protonation. Fig. 1 depicts the protonation dynamics of pyranine anion either in water (curve A) or in the presence of oxidized (curve B) or reduced Tuna cytochrome (curve C). In the absence of protein, the re-protonation of the anion is very fast with a time constant $\tau \sim 2$ μs. In the presence of cyto-

chrome *c*, we still observe the initial fast re-protonation of the dye. Yet, after a few μs, the reaction becomes slower by an order of magnitude. During the slow phase, the mechanism of pyranine re-protonation is through collisional proton abstraction from these protonated sites that just gained their proton a few μs before.

The experimental system used in this study ensured that the amount of released protons was less than the protein concentration. Thus only a few molecules of cytochrome *c* were protonated by a single proton on a random proton binding site. This limitation ensured that the total charge of each protein molecule was constant as the only charge increment was by the reacting proton. The low concentration of the protein also prevented any collisional proton transfer among the protein molecules. As a result, the only proton transfer reactions were the proton exchange among the various proton binding sites on the same protein molecule while its charge is constant. Comparison of the curves measured with the oxidized and reduced protein reveals that the reduced cytochrome *c* can better retain the proton from reacting with the pyranine. Detailed analysis of the kinetics [54] could determine the p*K* shift of surface carboxylates. The oxidation of the heme increased the positive charge of the protein causing a downshift of the p*K* values of all carboxylates that reacted with proton within the observation period. For some carboxylates, the measured p*K* shift was from 4.2 to 4.4 while others were shifted by as much as 0.5 units. Thus the dynamics measurements have a clear advantage in measuring the p*K* of a low p*K* residue without going down to the pH range where the protein looses its stability and without accumulation of excess charges on the protein during the process of the titration.

5. Proton transfer between nearby sites

Proton binding sites on a phospholipids membrane are packed at a density of a site $\sim$50–70 Å^2, comparable to inter-molecule separation of a $\sim$3–5 M homogeneous solution. On a protein, the carboxylate or histidine residues can attain even higher densities. The quantitation of the rates of proton transfer in such overcrowded solution can be measured as the rate of deprotonation of excited pyranine molecule in the presence of concentrated solution (up to 8 M) of acceptor like acetate. As the concentration of the acceptor increases, the mechanism of the reaction is changing. At a very low concentration of acetate, the rate-limiting step of the dissociation is the solvation of the products with a typical time constant of 120 ps [14–16]. As the acetate concentration approaches $\sim$50 mM, the classical proton transfer between the acetate (acceptor) and the excited pyranine (donor) became faster than the dissociation step and the reaction becomes a diffusion-controlled reaction. At higher concentrations of the acceptor (above 1 M), a new mechanism step becomes apparent as some acetate molecules are already at contact distance from the excited pyranine molecule. In that situation, the proton transfer to these molecules will be faster than the diffusional step and the rate-limiting step will be the net chemical step of the reaction, reaching an upper limit of $\tau\sim$2.5 ps [55,56].

Proton exchange among proton binding sites on bio-structures differs from the reaction in overcrowded solution by one major feature; in very concentrated solution, the proton is instantly taken up by the adjacent acetate molecules with no dispersion to the bulk. On the surface of a protein, or a membrane, the proton exchange reaction proceeds in close contact with the bulk which acts as another attractor.

There are two modes to quantitate the velocity of the reaction of proton exchange over packed clusters of proton binding sites on a bio-structure. One is a theoretical model based on the simulation of reversible proton dissociation where the basic model of geminate recombination is expanded to describe the dynamics of proton transfer from one site (donor) to the acceptor while the bulk operates as a second attractor. These calculations are based on molecular modeling and are suitable for a simplified system at vanishing ionic strength. The other method to study proton transfer among adjacent sites is to measure the dynamics of interaction with free proton and analyze the results by classical chemical rate equations. The gained mechanistic simplification of presenting a non-homogeneous dispersed by homogeneous one carries its own penalty. These rate constants are applicable for a virtual situation where the fixed proton binding sites are treated as free spices in homogeneous solution. Because of the virtual concen-

trations, the term M^{-1} s^{-1} unit is not relevant to these rate constants.

5.1. Reversible proton dissociation in a double well system

The dynamics of proton transfer between two adjacent sites can be analyzed using the program of Agmon for quantitating the geminate recombination reaction. The dissociation of a proton is described as a series of reversible steps of ion pair formation, solvation of the products and the diffusion of the proton within the electrostatic potential well made by the charge of the anion. The whole reaction is a product of probability terms that are used to propagate the diffusing proton over time and space until it equilibrates with the bulk [10,14,15].

The model can modulate to describe a proton transfer between two sites in the presence of bulk as another attractor. The discharged proton can either recombine with its parent molecule, with another anion placed at a given distance from the source or diffuse to the bulk. The scenario is terminated by any of the following states; the proton recombines with the origin site, it reacts with the next site or is lost to the bulk. In the first case, no proton exchange reaction takes place, the second one is regard as a successful proton transfer between adjacent sites and the third one corresponds with a normal dissociation where the nearby site had no effect on the path of the reaction. Under ideal conditions (zero ionic strength, no competing counterions), the probability of proton exchange among the sites was found to be a function of the separation distance. As long as the distance is smaller than the Coulomb cage radius, the efficiency to the exchange between the sites was close to 100%, with hardly a loss of protons to the bulk. As the distance increased, the probability dropped rapidly while the bulk became the dominant attractor.

A pair of exchanging sites can easily be expanded into a series of coupled sites arranged as a 'proton guide', which will let protons flow with minimal probability of dispersion to the bulk. The multi-site model is much more sensitive to the environmental conditions than a pair of sites. A sequential passage through a set of sites is a random walk process and the distance covered is a function of the square root of the number of steps ($R = \sqrt{n}$). On the other hand, the probability that the proton will be lost to the bulk is a function of n. Thus, as the conducting array is getting longer, its efficiency decreases. Another source for a loss of conductivity along the array is its extreme sensitivity to the presence of counterions; whenever a cation binds to the array, it will disrupt the continuity. A proton reaching an occupied site will be spilled to the bulk. As the main force keeping the proton from dispersing to the bulk is the electrostatic attraction, the guide system will loose its efficiency due to ionic screening. In $\sim$100 mM salt solution, where the Debye length is $\sim$10 Å, sites located more than that distance apart will not function as a part of the proton guide. It is evident from the present discussion that the proton guide can readily loose its efficiency due to a local loss of continuity. Consequently, a model should be looked for.

5.2. Virtual second order reaction

An alternative model for quantitation of proton transfer among nearby sites is to assume a virtual situation where the sites, actually fixed on a rigid scaffolding, can execute a 'collisional' proton exchange reaction among them. The correlation between concentrations and velocities, according to this model, is described by the virtual second order reaction. These values can be precisely quantitated but cannot be transformed into the familiar terminology of second order kinetics having the units of M^{-1} s^{-1}. In the virtual space, the reactive sites are assumed to be homogeneously distributed in the reaction space, while the assigned rate constants incorporate the actual connectivity between the reacting sites. Thus, for two sites which are located one within the Coulomb cage of the other, the virtual second order rate constant will be larger than for a well separated pair for which the efficient proton delivery is reduced. Bearing this limitation in mind, the presentation offers an opportunity to express the connectivity among sites by quantitative parameters that are self-consistent within the model.

The primary calibration of the virtual second order reaction was attained by studying the velocity of protonation of the chromophoric site of fluorescein derivatives where additional proton binding sites were attached to the dye's skeleton [57]. The rates

of the reaction of the dye with free protons were found to be within the limits set by the Debye Smulochovski equation for diffusion-controlled reactions. But, the rate constant for proton exchange between the sites on the dye molecule were exceptionally high, as much as 10^{12} M^{-1} s^{-1}. Such high rates imply that the reaction mechanism is not a collision between two dye molecules but rather a sequential dissociation of the proton from one site and rebinding by the next site on the very same molecule, before the proton is dispersed in the bulk. Thus the virtual rate constant reflects the same considerations that were discussed in the above section, using terminology of chemical kinetics. Comparison of virtual second order reaction between sites on the fluorescein skeleton revealed wide variation in the rate constants. This variation indicates that other terms like solvation shell and local electrostatic potential also affect the measured rate constants [57].

Marantz and Nachliel had demonstrated the analytic power of the model [54]. In their studies of the protonation dynamics of cytochrome *c*, they calculated the virtual second order reaction for the proton exchange among all surface groups of the protein in its oxidized and reduced states. The Tuna's cytochrome *c* was found to have five proton reactive carboxylates on its surface and a single histidine residue (H26). All these groups sustain a very inefficient proton exchange reaction among them ($k < 10^8$) except for the residues E44 and H26, which are less than 10 Å apart. For the reduced protein, the (virtual) rate constant of the reaction was $k = 10 \times 10^{10}$ while for the oxidized protein, the rate constant was four times smaller, $k = 2.5 \times 10^{10}$. Four-fold variation in the rate of the reaction implies that the protonic connectivity between the two sites had been modified, either due to relative motion of sites or to rearrangement of their solvation shell. Comparison of the three-dimensional model of cytochrome *c* (with a spatial resolution of 1.5 and 1.8 Å for the reduced and oxidized states, respectively) does not reveal major structural alteration in the E44–H26 region. The distance between the nitrogen atom of the imidazole ring of H26 to the carboxylate of E44 is slightly longer in the reduced state (8.1 Å) than in the oxidized protein (7.8 Å). Thus, the 4-fold modulation of the rate constant has to be attributed to the time dependent conformation of the protein, which is not expressed by the average structure of cytochrome *c*.

The high resolving methods like X-ray diffraction or NMR are slow scanning procedures that reflect the dominant, time-averaged, conformation. The fast proton transfer dynamics amplify the contribution of those conformations that have the highest rate of proton transfer, even if they consist only a small component of the whole conformations population (see also [58]). The fast proton exchange rate, inconsistent with the time-averaged structural data, implies that the flexibility of the E44 residue varies with the redox state of cytochrome *c*; When reduced, the probability that thermal flocculation will bring E44-H^+ to contact with H26 is higher than for the oxidized protein. Examination of the crystal structure data supports our conclusion. The *R* value of the oxygen atoms of the carboxylate moiety of E44 of the reduced protein is significantly larger than that of the oxidized one, while the imidazole ring has about the same *R* values in both redox states. The kinetic analysis sharpens the structural understanding of the protein by focussing on the dynamics of the protein, a parameter that could not detected by slow scanning methods.

6. Prediction of a long range proton transfer trajectory

Section 5 discussed the mechanism of proton transfer at a molecular level as a short range passage between adjacent sites or through a narrow channel that confined the proton in one-dimensional space. In the present section, we shall address the mechanism of proton transfer through a large space having tens of water molecules surrounded by low dielectric boundaries. The algorithm used for predicting the trajectory is similar to that used for the simulation of proton transfer between two attractors (see Section 5.1) except that the electrostatic potential is precisely calculated by the Delphi program. According to this approach, the electrostatic potential of the gauged space is first mapped by the Delphi program and the slope of the electrostatic potential is calculated. On that basis, a trajectory (or trajectories) is defined and the propagation of the proton is calculated. The system is iterated by changing the chem-

ical and physical characteristics of the system, until the predicted dynamics are superpositioned over the experimental one. In the present section, we shall discuss the trajectory of a proton within two confined spaces. The first is a simple model where the boundaries surrounding the aqueous phase are phospholipids. Later, the same procedure will be applied to utilize the proton pulse for gauging the inner space of the PhoE channel.

6.1. Proton transfer in Hex II

The Hex II packing of phospholipids [59,60] offers a simple system for the study of the diffusion of protons in a well defined geometry; 'infinitely' long tubes of phospholipids (PC and PE) with a pre-calibrated diameter. The insertion of pyranine into the Hex II system offers the opportunity to monitor the dynamics of a proton diffusion, in uncharged structures, under no external force. The Hex II structures were formed by swelling of the lipids in a dilute pyranine solution and the dynamics of the reversible photo-dissociation were measured by time-resolved fluorescence ([60], Fried, Ph.D. thesis).

The steady state fluorescence of the pyranine locked in the Hex II system was characterized by two emission peaks: 440 nm and 550 nm, the radiative decay of the un-dissociated species pyranine (ΦOH*) and the radiative decay of the anion (ΦO^-*), respectively. In water, pH = 5, the ratio of the emissions is about 0.05 but inside the Hex II, the ratio increased to 0.3–0.5 depending on the radius of the tube. This enhanced emission of the un-dissociated molecule implied an enhanced stability of ΦOH*. The time-resolved fluorescence of the pyranine, at the wavelength of ΦOH*, exhibits a non-exponential decay curve. At the first 200 ps, there are fast kinetics which slowed down with time. This pattern corresponds with a complex dissociation process; not only that the ejection of the proton to the solvent is slower than in bulk water, but the dispersion of the proton to the bulk is slowed by intensive attraction of the proton towards the pyranine anion.

Quantitation of the rate constants and the electrostatic forces operating on a proton inside the Hex II tubes was based on analysis of the fluorescence decay curves measured for pyranine molecules locked in the aqueous phase of Hex II preparation [14–16,60]. The Hex II structures were prepared under conditions where their radii varied from 15 to 27 Å, and the dynamics of dissociation of the excited pyranine were measured and analyzed. The analysis was based on numeric propagation, in time and space, of the ejected proton. The reaction can be divided into two spatial domains. The first one is taking place on the surface of the pyranine reaction sphere where the proton is reversibly ejected and re-absorbed. The rate constants at the surface of the reaction sphere reflect the activity of the water in the vicinity of the anion and the stability of the solvated proton and control the first 2 ns. The second domain extends from the surface of the reaction sphere and on. In this domain, the proton diffuses against the electrostatic attraction of the parent anion (ΦO^-*) while being attracted outwards by entropic. The process is reminiscent of the diffusion in a double well system (see Section 5.1) (for details, see [13–16,19,24,60]).

Detailed analysis of the results indicated that the activity of the water, as gauged by the initial rate of the dissociation dynamics, was constant ($a_{water} = 0.84 \pm 0.05$) over the measured range of the tube's radii. This constancy implied that in all samples, the pyranine molecule was located in the same loci, i.e. at the water lipid interface. This conclusion is in accord with the known tendency of pyranine to adsorb on uncharged phospholipid surfaces [24,61].

Once the location of the dye within the tube was established, the electrostatic map could be calculated. The Hex II structure was assembled by the Insight program using the phospholipids membrane model of Peitzsch et al. [62]. The pyranine anion ($q = -4$), represented by a sphere with a reaction radius of 6 Å, was placed at the inner surface of the close shape structures and the electrostatic potential of the aqueous space within the cylinder was calculated by the Delphi program.

Fig. 2 depicts electrostatic potentials in the presence of the pyranine anion in the tube. A schematic description of the trajectory is inserted in the figure. Right next to the pyranine anion, at the surface of the anion's reaction sphere, the potential of the proton is −11.5 kT. Yet with the increase distance between the positive charge and the anion, the potential becomes less negative, as indicated by the two curves shown in the figure. Curve A, originating from the reaction sphere, depicts the variation of

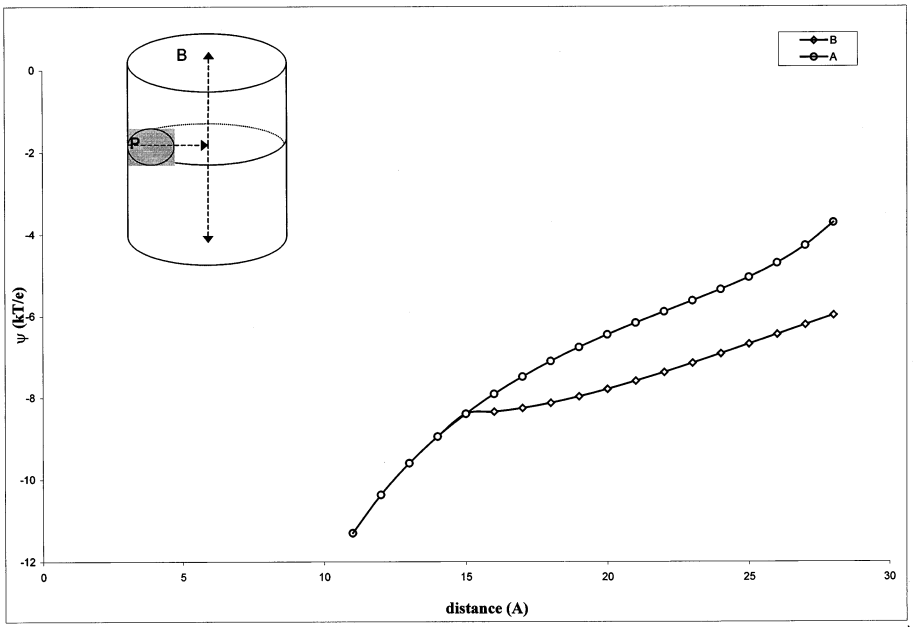

Fig. 2. The changing of the electrostatic potential within a Hex II tube with a diameter of 30 Å. The pyranine anion, having a reaction radius of 6 Å [14], was placed in contact with the phospholipid headgroups and the potential for a free proton is calculated initiating at 12 Å from the inner surface of the tube. Curve A depicts the variation of the potential as the proton propagates along the radius vector on the plane towards the other side of the tube. Curve B initiates from the center point of the cross section of the tube and describes the potential of the proton as it propagates vertically along the long axis of the tube. The inset depicts the two trajectories corresponding with curves A and B.

the electrostatic potential as the proton diffuses on the surface of the XY plan where the pyranine is located. As the slope of the potential curve decreases, the proton propagates away from the pyranine and the dispersion to space will become more attractive. As the proton's charge crosses the axis, its electrostatic potential is influenced by the dielectric boundary of the opposite wall and the slope of curve A increases again. From that point and on, the more favorable trajectory will be along the Z axis (curve B) located at the center of the tube.

The spontaneous pathway taken by a proton ejected from the pyranine will follow the route of the minimal electrostatic gradient. Thus it will first diffuse on the XY plan, later along the Z axis. This trajectory is independent of the dielectric constant of the aqueous phase, but not the actual values of the electrostatic potential. Both the magnitude and the slope will vary with ε_{water}. To determine the dielectric constant of the aqueous phase, the potential gradient, as in Fig. 2, was calculated for a wide range of ε_{water} values and tested for its capacity to reconstruct the measured fluorescence decay curves of the excited pyranine molecule. The dynamics could be fitted in a satisfactory way only when the dielectric constant of the water in the tube was set to be less than 80. What more, the value varied with the tube's radius. As the radius of the tube increases from 15 Å to 24 Å, the fittings were attained with the dielectric constant of the aqueous phase increasing from $\varepsilon_{water} = 40$ to $\varepsilon_{water} = 55$. In parallel, the diffusion coefficient of the protons increased from 7.6×10^{-6} up to 2×10^{-5} cm^2 s^{-1}.

6.2. Proton diffusion in the PhoE channel

Ion channels like the porin or the VDAC are large-pore β-barrel structures. The inner space of the channel is uneven in shape, where one of the loops (L3) extends into the pore generating a constriction zone [63]. Studies with site specific mutations indicated that insertion of bulky or charged groups near the eyelet appears to control the rate and selectivity of the ion flux [64–67]. The correlation between the structural modifications and the conductivity of the channel was analyzed on the assumption that the rate-limiting step of ion passage is at the eyelet [66,68,69].

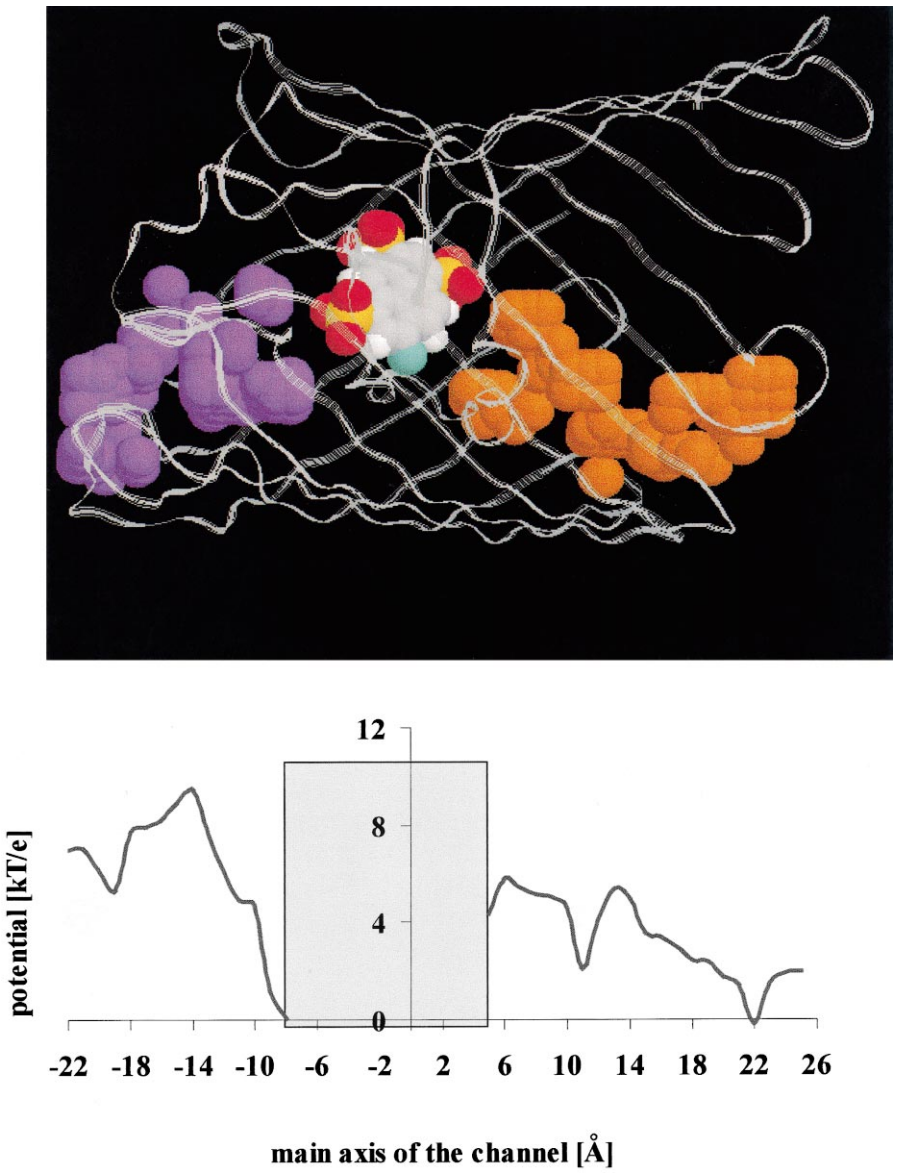

Fig. 3. The electrostatic potential within the aqueous space of the PhoE pyranine complex channel. The model was based on the structure of the protein (PDB entry: 1PHOE) and the pyranine molecule is located in the most stable site within the channel. The hydroxyl moiety of the pyranine is colored green while the sulfono residues are marked by an arrow. The protein matrix was assigned with $\varepsilon = 2$ and the aqueous phase in the channel with $\varepsilon_{water} = 50$. The electrostatic potential was calculated using the Delphi program of MSI using the partial charges given by PARSE [72]. The intra-channel space is represented by a 1 Å grid and trajectory is marked by colored spheres. In slices where the potential well is shallow, the trajectory expands and in a few cases seems to diverge. In the lower part of the figure, the electrostatic potentials along the trajectory are presented. The gray area, on both sides of the pyranine, defines the space within the reaction sphere. The potential calculated at the surface of the pyranine reaction sphere, facing the extracellular section, was arbitrarily set as zero.

On the other hand, we have to consider that for a system characterized by high throughput, the overall flux is seldom controlled by a single rate-limiting step. Potential along the whole length of the channel, including also the vestibule 301, will form a sequence of barriers and potential wells. Thus, by calculating the propagation of a charged particle along a trajectory, characterized by a given electrostatic profile, a realistic ion flux can be predicted. The key point in these calculations will be the value of the dielectric

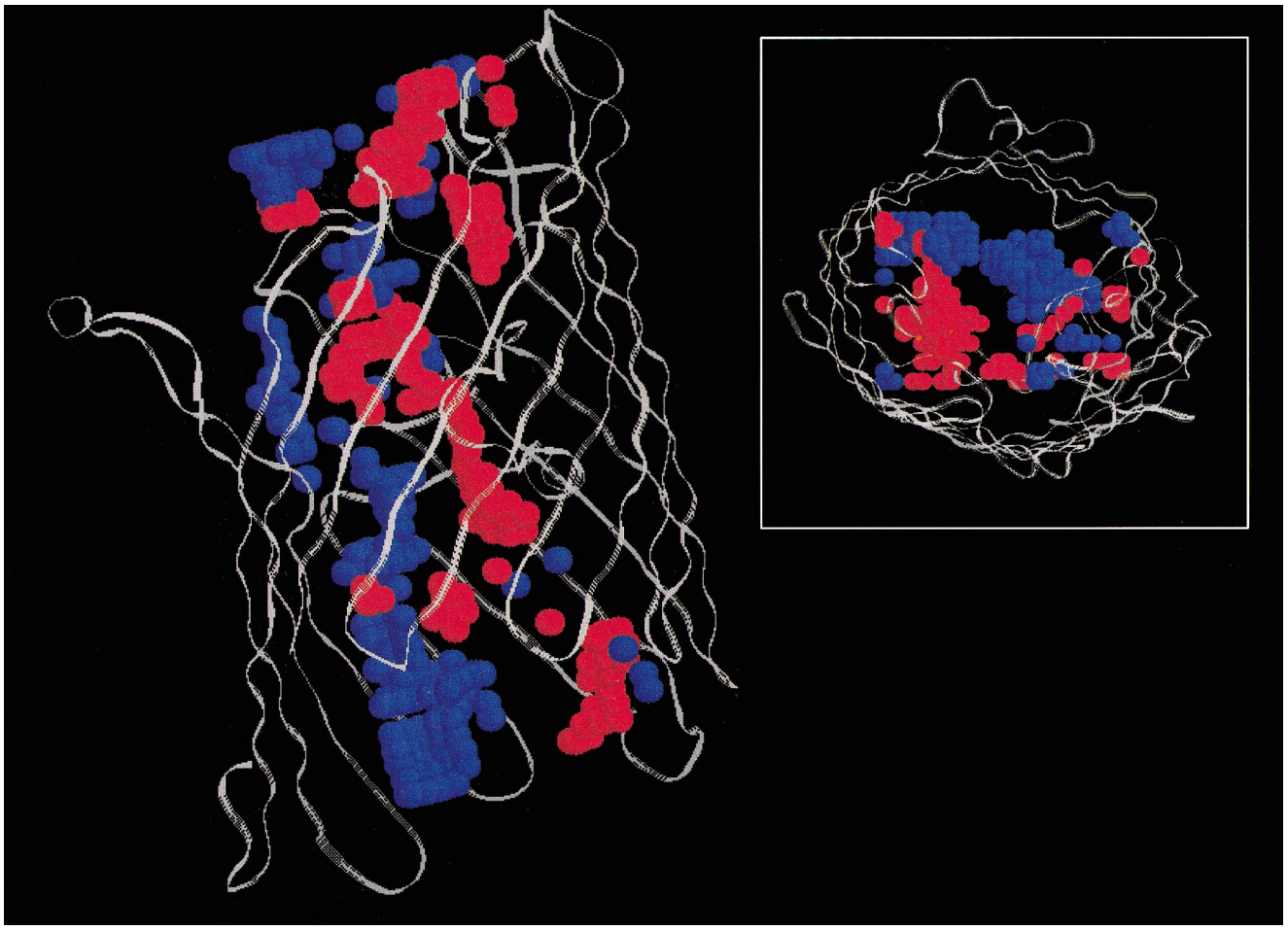

Fig. 4. The trajectory of anion (red) and cation (blue) through the PhoE channel. The potentials were calculated by the Delphi program on the basis of the structure (PDB entry: 1PHOE) using the partial charges given by PARSE [72]. Please note that the two trajectories are avoiding each other adhering to the protein water interface. The periplasmic sides of the enzyme are at the bottom of the figure. The inset depicts the bipolar distribution of charges as seen along the Z axis.

constant assigned to the water in the cavity. Karshikoff et al. [70] had calculated the electrostatic potential along the PhoE channel and pointed out that the field varies along the length of the channel, both in intensity and in polarity. Their calculations were based on the approximation $\varepsilon_{water} = 80$, in contrast with the theoretical estimation of Sansom et al. [71] who reasoned that inside a β-barrel, $\varepsilon_{water} \sim 40$. Thus a direct determination of the ε_{water} is required.

Gutman et al. [19] analyzed the dynamics of the fluorescence decay of pyranine in the PhoE channel and deduced, on the basis of a schematic structure, an apparent dielectric constant of $\varepsilon_{app} = 24$. Recently, Bransburg-Zabary (Ph.D. thesis) used the 2.4 Å structure (PDB entry: 1PHOE) to calculate by the Delphi program the intra-cavity potential map of the PhoE. On the basis of these calculations, the fluorescence decay of the pyranine was analyzed and the dielectric constant of the water in the PhoE channel and found to be $25 \leq \varepsilon \leq 50$.

The trajectory of proton transfer within the PhoE channel, in the presence of pyranine, is shown in Fig. 3. The intra-channel aqueous space is represented as white dots separated by 1 Å where those on the trajectory are marked by colored 1 Å spheres. The trajectory extends from the surface of the pyranine reaction sphere [13–16] all the way to both edges of the channel. As can be seen, the two trajectories take only a small fraction of the total volume of the channel and are neither straight nor continuous lines. In some of the slices along the Z axis, the trajectories appear to have more than one region of preference,

representing a local attractor that diverges from the main path.

The electrostatic potentials along these trajectories are given at the bottom of Fig. 3. The trajectory on the extra-cellular site has a lower potential reflecting the contribution of the two SO_3^- residues (marked by arrows). This point was taken as the reference and its electrostatic potential was defined as zero. The potential in the periplasmic section is higher than of the extra-cellular one by $\sim$5 kT/electron and its profile is rather shallow. The propagation of the proton in each section of the channel is determined by the gradient of the electrostatic potential. Thus the periplasmic section will offer a faster trajectory than the extra-cellular one. Yet the initial difference in the electrostatic potentials may favore the escape through the extra-cellular route. The shallow profile of the periplasmic section hardly offers any resistance to the escape of the proton and the expected rate of proton escape is much faster than the measured one. Thus both the kinetics and the thermodynamic calculations negate the periplasmic section as the one from which the proton, ejected by the excited pyranine, will select. The steep electrostatic gradient along the extra-cellular section offers a retarding force that slows the calculated rate of escape, making it compatible with the measured dynamics.

On the basis of the results with the pyranine, we calculated the trajectory for cations and anions through the channel. Fig. 4 depicts the trajectory of positive (blue) and negative (red) charges (from the extra-cellular to the periplasmic sides of the PhoE). As seen in the figure, each species will progress in a tortuous pathway. The trajectories are avoiding each other close to the water–protein interface where the effect of the fixed charges is maximized. The flux of the ions along the predicted trajectories is within the order of magnitudes of those measured for the PhoE, thus corresponding with a real simulation of the currents within the channel.

7. Concluding remarks

The propagation of proton through channels in proteins proceeds along pathways made of proton binding sites interconnected by water molecules. The rate and efficiency proton transfer between these elements depend on the physical chemical properties of the reacting species. The most crucial parameters are the connectivity between the sites and the gradient of the electrostatic potential along the route. At present, the precise molecular dynamic modeling of a proton passage through a channel cannot be attained. For this reason, a quantitative evaluation of the mechanism has to be based on chemical dynamics which simulate the reaction through propagation in time and space of the proton along the whole system. One way of deriving the reaction is based on detailed molecular information like the distance between the sites and the local electrostatic potential. An alternative method transforms the reaction into a virtual space where fixed sites can interact with each other by virtual second order reaction. While each mode of quantitation has its inherent limitations, the application of both can yield a higher level of information.

There are two crucial elements for a long range intra-protein proton transfer. One is the connectivity between all elements of the pathway. The connectivity should not be permanently excising. Under favorable conditions, the rate of proton transfer can be so high that even transient connectivity can suffice to bridge between proton binding sites, rendering them elements of a conductive pathway. The other parameter controlling the long range proton transfer is the electrostatic potential. The frequency at which a proton is probing its immediate environment is extremely high. Thus even that an energy barrier of 4–5 kT/e will reduce the fraction of attempts to surmount the barrier to $\sim$1%. Within the time scale of enzymic, the proton passage may take place. Thus the electrostatic regulation of proton transfer is mediated not only by the height of the barrier but also by its gradient (kT/Å).

In the case of narrow, single file conducting path, the tracing of the line of propagation is rather simple. In large spaces where tens (or hundreds) of water molecules are grouped together, the proton will follow an explicit (yet tortuous) trajectory that overlaps the path of minimal electrostatic resistance. The same rule applies to the diffusion (or flux under external electrostatic field) of other ions. The control over flux and the chemical selectivity encountered by various ion-transporting proteins is based on the same rules that govern the passage of protons.

Acknowledgements

The research in the Laser Laboratory for Fast reactions in Biology is supported by research Grant of the American-Israeli Bi-National Science Foundation (97-00130), German Israel Science foundation (I054-140.09/98) and Volkswagen Stiftung (I/72 867).

References

[1] N. Friedman, I. Rousso, M. Sheves, X. Fu, S. Bressler, S.O.M. Druckmann, Biochemistry 36 (1997) 11369–11380.
[2] X. Fu, S. Bressler, M. Ottolenghi, T. Eliash, N. Friedman, M. sheves, FEBS Lett. 416 (1997) 167–170.
[3] J.K. Lanyi, J. Biol. Chem. 272 (1997) 31209–31212.
[4] M. Gutman, E. Nachliel, Biochim. Biophys. Acta 1015 (1990) 391–414.
[5] M. Gutman, E. Nachliel, Annu. Rev. Phys. Chem. 48 (1997) 329–356.
[6] M. Gutman, Methods Biochem. Anal. 30 (1984) 1–103.
[7] M. Gutman, Methods Enzymol. 127 (1986) 522–538.
[8] M. Gutman, A.B. Kotlyar, N. Borovok, E. Nachliel, Biochemistry 32 (1993) 2942–2946.
[9] S. Checover, E. Nachliel, N.A. Dencher, M. Gutman, Biochemistry 36 (1997) 13919–13928.
[10] M. Gutman, E. Nachliel, Biochim. Biophys. Acta 1015 (1990) 391–414.
[11] M. Gutman, E. Nachliel and Y. Tsfadia, in: E.A. Disalvo and S.A. Simon (Eds.), Permeability and Stability, CRS Press, 1995, pp. 259–276.
[12] J.F. Irland, P.A.H. Wyatt, Adv. Phys. Org. Chem. 12 (1976) 131.
[13] E. Pines, D. Huppert, N. Agmon, J. Chem. Phys. 88 (1988) 5620–5630.
[14] N. Agmon, E. Pines, D. Huppert, J. Chem. Phys. 88 (1988) 5631–5638.
[15] N. Agmon, J. Chem. Phys. 88 (1988) 5639–5642.
[16] E. Pines, G.R. Fleming, J. Chem. Phys. 95 (1991) 10448–10457.
[17] R. Yam, E. Nachliel, M. Gutman, J. Am. Chem. Soc. 110 (1988) 2636–2640.
[18] E. Shimoni, Y. Tsfadia, E. Nachliel, M. Gutman, Biophys. J. 64 (1993) 472–479.
[19] M. Gutman, Y. Tsfadia, A. Masad, E. Nachliel, Biochim. Biophys. Acta 1109 (1992) 141–148.
[20] M. Gutman, E. Nachliel, D. Huppert, Eur. J. Biochem. 125 (1982) 175–181.
[21] M. Gutman, E. Nachliel, Solid State Ionics 61 (1993) 229–234.
[22] R. Yam, E. Nachliel, S. Kiryati, M. Gutman, D. Huppert, Biophys. J. 59 (1991) 4–11.
[23] A.B. Kotlyar, N. Borovok, S. Kiryati, E. Nachliel, M. Gutman, Biochemistry 33 (1994) 873–879.
[24] M. Gutman, E. Nachliel, S. Kiryati, Biophys. J. 63 (1992) 281–290.
[25] J. Fitter, S.A.W. Verclas, R.E. Lechner, H. Seelert, N.A. Dencher, FEBS Lett. 433 (1998) 321–325.
[26] D.A. Mills, M.S. Ferguson, Biochim. Biophys. Acta 1365 (1998) 46–52.
[27] P. Brzezinski, P. Adelroth, J. Bioenerg. Biomembr. 30 (1998) 99–107.
[28] M. Wikstrom, J.E. Morgan, M.I. Verkhovsky, J. Bioenerg. Biomembr. 30 (1998) 139–145.
[29] N. Agmon, J. Mol. Liquids 64 (1995) 161–195.
[30] H. Leuchs, G. Zundel, Can. J. Chem. 60 (1982) 2118–2131.
[31] G. Zundel, J. Mol. Struct. 322 (1994) 33–42.
[32] F. Stillinger, in: H. Eyring and D. Henderson (Eds.), Theoretical Chemistry Advances and Prespective, Academic press, New York, 1978, pp. 177–234.
[33] E. Nachliel, M. Gutman, L. Even Zohar, Solid State Ionics 77 (1995) 79–83.
[34] D.E. Sagnella, G.A. Voth, Biophys. J. 70 (1996) 2043–2051.
[35] R. Pomes, B. Roux, Biophys. J. 71 (1996) 19–39.
[36] R.T. Mathias, G.J. Baldo, K. Manivannan and S. McLaughlin, in: R. Guidelli (Eds.), Electrified Interfaces in Physics Chemistry and Biology, Kluwer academic publishers, 1992, pp. 473–490.
[37] P. Maroti, Biophys. J. 73 (1997) 367–381.
[38] E.C. Abresch, M.L. Paddock, M.H.B. Stowell, T.M. Mcphillips, H.L. Axelrod, S.M. Soltis, D.C. Rees, M.Y. Okamura, G. Feher, Photosynth. Res. 55 (1998) 119–125.
[39] J.L. Li, D. Gilroy, D.M. Tiede, Biochemistry 37 (1998) 2818–2829.
[40] M.L. Paddock, G. Feher, M.Y. Okamura, Biochemistry 36 (1997) 14238–14249.
[41] P. Brzezinski, M.L. Paddock, M.Y. Okamura, G. Feher, Biochim. Biophys. Acta 1321 (1997) 149–156.
[42] B. Rabenstein, G.M. Ullmann, Biochemistry 37 (1998) 2488–2495.
[43] G. Fritzsch, L. Kampmann, G. Kapaun, H. Michel, Photosynth. Res. 55 (1998) 127–132.
[44] J. Miksovska, P. Maroti, J. Tandori, M. Schiffer, D.K. Hanson, Biochemistry 35 (1996) 15411–15417.
[45] P. Maroti, C.A. Wraight, Biochim. Biophys. Acta 934 (1988) 314–328.
[46] P.H. McPherson, M.Y. Okamura, G. Feher, Biochim. Biophys. Acta 934 (1988) 348–368.
[47] P.H. McPherson, M.Y. Okamura, G. Feher, Biochim. Biophys. Acta 1144 (1993) 309–324.
[48] P. Beroza, D.R. Fredkin, M.Y. Okamura, G. Feher, Biophys. J. 68 (1995) 2233–2250.
[49] C.R. Lancaster, H. Michel, B. Honig, M.R. Gunner, Biophys. J. 70 (1996) 2469–2492.
[50] D.K. Hanson, Photosynth. Res. 55 (1998) 275–280.
[51] J. Miksovska, L. Kalman, M. Schiffer, P. Maroti, P. Sebban, Biochemistry 36 (1997) 12216–12226.
[52] P. Sebban, P. Maroti, M. Schiffer, D.K. Hanson, Biochemistry 34 (1995) 8390–8397.

[53] M.S. Graige, G. Feher, M.Y. Okamura, Proc. Natl. Acad. Sci. USA 95 (1998) 11679–11684.
[54] Y. Marantz and E. Nachliel (1999) Isr. J. Chem. (in press).
[55] D. Huppert, L. Tolbert, s. Linares-samaniego, J. Phys. Chem 101 (1997) 4602–4605.
[56] M.K. solntsev, D. Huppert, L. Tolbert, N. Agmon, J. Am. Chem. Soc. 120 (1998) 7981–7982.
[57] V. Sacks, Y. Marantz, A. Aagaard, S. Checover, E. Nachliel, M. Gutman, Biochem. Biophys. Acta 1365 (1998) 232–240.
[58] J.F. Calvert, J.L. Hill, A. Dong, Arch. Biochem. Biophys. 346 (1997) 287–293.
[59] R. Rand, N.L. Fuller, S.M. Gruner, V.A. Parsegian, Biochemistry 29 (1990) 76–87.
[60] O. Fried, E. Nachliel, M. Gutman, Solid State Ionics 77 (1995) 84–88.
[61] N.R. Clement, J.M. Gould, Biochemistry 20 (1981) 1534–1538.
[62] R.M. Peitzsch, M. Eisenberg, K.A. Sharp, Biophys. J. 68 (1995) 729–738.
[63] S.W. Cowan, T. Schirmer, G. Rummel, M. Steiert, R. Ghosh, R.A. Pauptit, Nature 358 (1992) 727–733.
[64] E.F. Eppens, N. Saint, P. Van-Gelder, R. van-Boxtel, J. Tommassen, FEBS Lett. 415 (1997) 317–320.
[65] P. Van-Gelder, N. Saint, R. van-Boxtel, J.P. Rosenbusch and J. Tommassen, Protein Eng. (1997) 699–706.
[66] B. Schmid, L. Maveyraud, M. Kromer and G.E. Schulz, Protein Sci. (1998) 1603–1611.
[67] P.S. Phale, T. Schirmer, A. Prilipov, K.L. Lou, A. Hardmeyer, Proc. Natl. Acad. Sci. USA 94 (1997) 6741–6745.
[68] D.P. Tieleman, H.J. Berendsen, Biophys. J. 74 (1998) 2786–2801.
[69] O.S. Smart, J. Breed, G.R. Smith, Biophys. J. 72 (1997) 1109–1126.
[70] A. Karshikoff, V. Spassov, S.W. Cowan, R. Ladenstein, T. Schirmer, J. Mol. Biol. 240 (1994) 372–384.
[71] M.S. Sansom, G.R. Smith, C. Adcock, P.C. Biggin, Biophys. J. 73 (1997) 2404–2415.
[72] D. Sikoff, N. Ben-Tal, B. Honig, J. Phys. Chem. 100 (1996) 2744–2752.